Computer Simulations of Hyperbranched Polymers: the Influence of the Wiener Index on the Intrinsic Viscosity and Radius of Gyration

Document Version:
Publisher's PDF, also known as Version of Record (includes final page, issue and volume numbers)

Please check the document version of this publication:

• A submitted manuscript is the version of the article upon submission and before peer-review. There can be important differences between the submitted version and the official published version of record. People interested in the research are advised to contact the author for the final version of the publication, or visit the DOI to the publisher's website.
• The final author version and the galley proof are versions of the publication after peer review.
• The final published version features the final layout of the paper including the volume, issue and page numbers.
Link to publication

Computer simulations of hyperbranched polymers: The influence of the Wiener index on the intrinsic viscosity and radius of gyration

Peter F. Sheridan and David B. Adolf[a]
IRC in Polymer Science and Technology, Department of Physics and Astronomy, University of Leeds, Leeds LS2 9JT, United Kingdom

Alexey V. Lyulin
Department of Applied Physics and Dutch Polymer Institute, Technische Universiteit Eindhoven, P.O. Box 513 5600 MB Eindhoven, The Netherlands

Igor Neelov and Geoffrey R. Davies
IRC in Polymer Science and Technology, Department of Physics and Astronomy, University of Leeds, Leeds LS2 9JT, United Kingdom

The influence of the Wiener index on solution properties of trifunctional hyperbranched polymers has been investigated using Brownian dynamics simulations with excluded volume and hydrodynamic interactions. A range of degrees of polymerization (N) and degrees of branching (DB) were used. For each DB and N, several molecules with different Wiener indices (W) were simulated, where W depends on the arrangement of branch points. The intrinsic viscosity and the radius of gyration (R_g) of HPs were both observed to scale with W at a constant N via a power law relationship, as found in the literature. Through their relationships to W, an expression relating intrinsic viscosity to R_g was obtained. This relationship is found to fall centrally between the predictions of Flory and Fox for linear polymers and that of Zimm and Kilb for branched polymers. Molecular shape in solution is also found to depend on W and N, as observed through the W dependence of the ratio of R_g to the hydrodynamic radius, R_h.   © 2002 American Institute of Physics. [DOI: 10.1063/1.1507774]

I. INTRODUCTION

Molecular structural control has provided a wealth of new polymer properties in recent decades. Since the 1980s, highly branched dendrimer and hyperbranched polymers (HPs) have generated increasing interest as the search for new polymer properties intensifies.[1–4] In general, these molecules possess a recursively branched, treelike structure. In a dendrimer, repeat units are concentrically layered around a focal core to create a unique structure for a given degree of polymerization, N. A layer within a dendrimer is also called a generation. The degree of branching (DB) is defined such that for a dendrimer DB is 1 (completely branched) and for a linear polymer DB is 0. The DB of HPs lies between 0 and 1,[4] higher values of DB indicating a more compact structure. Dendrimers' compact structure leads to remarkable properties. For a given N, low solution viscosities are measured for dendrimers relative to their linear counterparts and dendrimer intrinsic viscosities ([η]) are observed to reach a maximum and decrease with increasing generation number[1,5] which earmarks them as viscosity modifiers. Not surprisingly, dendrimers are expensive to synthesize due to the requisite number of protection/deprotection steps required within their fabrication. Relaxing these controlled chemistry protocols allows the creation of HPs from a one-pot synthesis. These reactions are more cost effective than dendrimer

syntheses and adapt well to large-scale production but offer a final product that is doubly polydisperse in N and DB. A key question surrounding the use of HPs is the extent to which they are able to mimic desired dendrimer properties. Examples within the literature reveal varied behavior. In one case,[6] irregular HPs were reported to show a dendrimerlike peak in [η] with increasing degree of polymerization (N). Within other efforts, a monotonic increase of [η] with N more akin to the Mark–Houwink behavior of linear polymers was observed, regardless of the degree of branching.[7–10] The conflicting message of these measurements may in part be due to the difficulty associated with characterizing these materials using size exclusion chromatography (SEC). The noted polydispersities in N and DB complicate the interpretation of SEC applied to HPs since a highly branched molecule with a large value of N can have the same hydrodynamic volume as a less branched or linear molecule with a smaller value of N.

Computer simulations offer further insight into the solution properties of branched molecules due to the ability to study the static and dynamic behavior of individual molecules with known N and DB values. Several simulation studies of HPs have been carried out to investigate [η] for dendrimers and HPs. Aerts used the kinetic bead-rod model of Lescanec and Muthukumar,[11,12] Widmann and Davies performed RIS metropolis Monte Carlo (RMMC) simulations of phantom chains in the absence of solvent,[13] while Lyulin *et al.* used Brownian dynamics (BD) with hydrodynamic in-

---

[a]Author to whom correspondence should be addressed. Electronic mail: d.b.adolf@leeds.ac.uk

DENDRIMER,

HYPERBRANCHED STRUCTURES BASED ON
DENDRIMER OF THE INDICATED GENERATION, g.

g = 3

g = 3

N = 46
DB = 1.00
W = 5661

N = 70
DB = 0.65
W = 15957

N = 67
DB = 0.68
W = 19332

g = 4

g = 4

N = 94
DB = 1.00
W = 31293

N = 166
DB = 0.56
W = 130725

N = 115
DB = 0.81
W = 70788

g = 5

g = 5

N = 190
DB = 1.00
W = 160893

N = 358
DB = 0.53
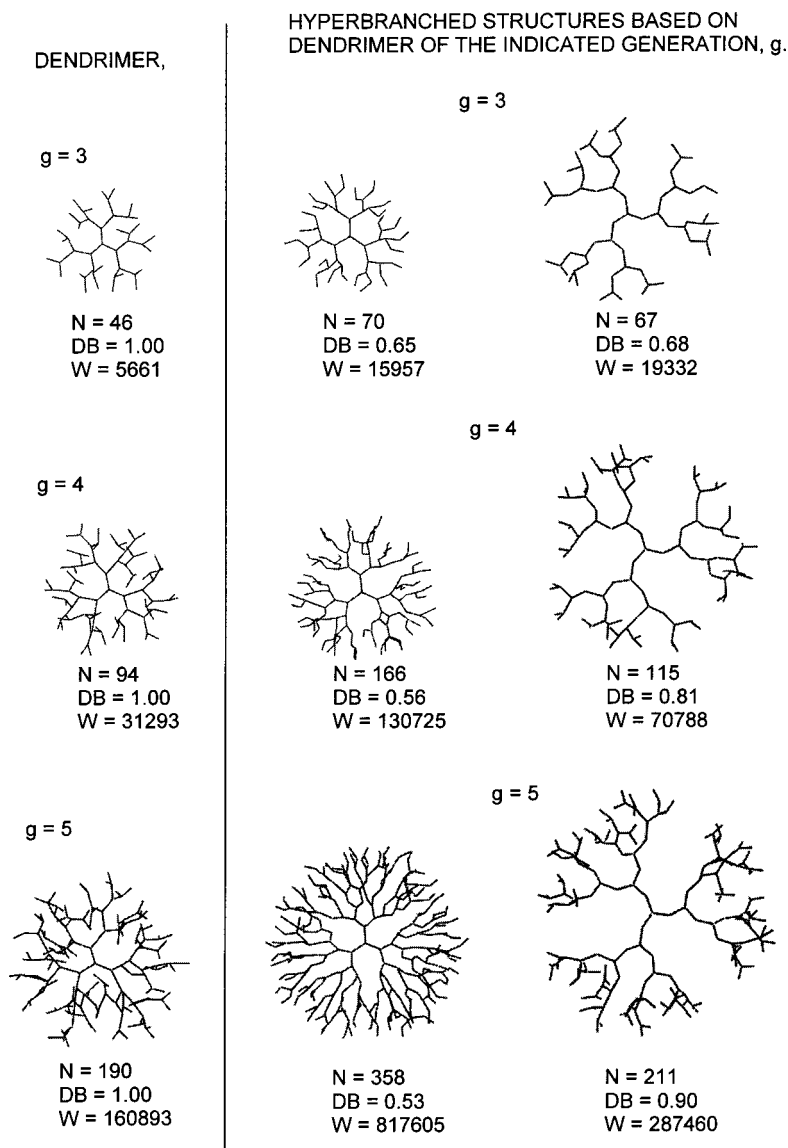W = 817605

N = 211
DB = 0.90
W = 287460

FIG. 1. Structures of six of the twelve symmetric hyperbranched molecules (HPs) simulated, labeled with degree of polymerization, N, degree of branching, DB, and Wiener index, W. These are based on dendrimers of generations 3, 4 and 5, which are pictured on the left for comparison.

teractions and excluded volume.[14] In each case, the authors simulated several families of HPs and, in addition, a family of linear molecules of increasing molecular weight and a family of dendrimers of increasing generation. Each HP family was composed of molecules with a constant DB (<1), but with the same increasing N values as the dendrimers. This facilitated comparisons of the HPs with the dendrimers and linear molecules. All these efforts revealed a dendrimerlike maximum in $[\eta]$ with increasing N for the highest DB family (the most compact HPs). A shallowing or disappearance of the peak was observed for HPs with decreasing DB. This behavior suggests DB as an effective index to distinguish different $[\eta]$ behaviors of HPs on a qualitative basis. However, DB only accounts for the relative number of branch points and is insensitive to their distribution within the molecule. The Wiener index, W, is a more suitable descriptor to employ when increased topological sensitivity is desired and possesses established links with molecular properties. The wide range of W values possible for branched structures with the same value of N and DB attests to its enhanced resolution in structural characterization.

The index was introduced by Wiener in 1947 and was found to correlate with the boiling points of alkanes.[15] Since then, it has been found to correlate closely with bulk refractive index, density, viscosity, melting point, boiling point, and surface tension of hydrocarbons,[16,17] and specific π-electronic energies and energy gaps of conjugated polymers.[18] W also correlates reasonably with refractive index, density, melting point, and specific rotation of various chain chemistries with vinyl additions[18] and has been linked to the surface-to-volume ratio of molecules, implying a further correlation with molecular interactions.[19]

The W value of a molecule is calculated as the cumulative sum of bond lengths along the shortest paths between all distinct pairs of units in the molecule. W is a direct measure of molecular compactness.[20] Converse to DB, W is lower for more compact molecules at a given N with more sprawled out, linearlike structures having higher W values at a given N. Widmann and Davies[13] and Lyulin *et al.*[14] calculated Wiener indices for the molecules they simulated. At a given degree of polymerization Widmann and Davies reported that $[\eta] \sim W^a$, where $a = 2.1$ to 2.7 with a increasing as N de-

creased. Lyulin *et al.* also obtained a power law relationship where $a=1.1$ to 1.6 following the same trend of a with N. Since the $[\eta]$ values of Widmann and Davies are calculated directly from simulated R_g's through the assumption that $[\eta] \sim R_g^3$, it can be seen that their RMMC simulations indicate $R_g \sim W^c$, where $c=0.7$ to 0.9. Analytical treatments exist for correlations of the radius of gyration, R_g, and $[\eta]$ with W. Bonchev *et al.*[21] and others[13,22] derived a power law of the form $R_g \sim W^{0.5}$ for branched ideal chains. Further analytical efforts[13] revealed a scaling of $[\eta] \sim W^{1.5}$, assuming $R_g \sim W^{0.5}$ and the relationship $[\eta] \sim R_g^3$. Widmann and Davies' exponents from RMMC were larger than these. They attributed this to their use of a simple simulated model of phantom chains without solvent and hydrodynamic interactions (HI).

Other theoretical studies of the solution properties of polymers have resulted in a direct relationship between $[\eta]$ and R_g. These approaches focus on particular architectures, rather than applying a general quantitative measure of topology such as W or DB. Flory and Fox derived a relationship for linear polymers in a θ-solvent,[23]

$$[\eta] = \Phi(6^{3/2}) R_g^3 M^{-1}, \qquad (1.1)$$

where M is the molecular weight and Φ was originally considered a universal constant. For branched molecules, Φ deviates from the ideal linear polymer value and varies strongly depending on the type and the extent of branching and molecular weight.[24–29]

A theoretical treatment due to Zimm and Stockmayer focused on the parameter g defined as the ratio of the squared radius of gyration of a branched polymer to that of a linear polymer of the same molecular weight, in θ-solution.[30] Zimm and Kilb introduced g' defined as the ratio of $[\eta]$ of a branched polymer to that of a linear polymer in θ-solution at the same molecular weight. Incorporating hydrodynamic interactions into the derivation of $[\eta]$ via the Kirkwood–Risemann approximation, they found that $g' \approx g^{0.5}$ for a star polymer model.[31] They proposed this applies to all molecular architectures, and found agreement with measurements of branched styrene-divinylbenzene copolymers.[31] Previously, Thurmond and Zimm used Eq. (1.1) to model the intrinsic viscosity of branched polymers,[32] in which case the relationship between contraction factors is $g' = g^{1.5}$. This approach was less successful in achieving agreement with experimental data on branched polymers than the result of Zimm and Kilb.[31,32] Experimental measurements of molecular weight (M), $[\eta]$, and R_g have since allowed the determination of relationships between g and g'. Exponents between 0.5 and 1.0 have been measured for various star polymers in different solvents.[29,33] For long chain branched polyethylene (LCB PE), Meira[34] suggests a general value 1.2 ± 0.2. However, an exponent of 2.0 has been measured.[35] Dependence of the exponent on molecular weight has also been observed for LCB PE, where measured exponents fall from 1.0 to 0.5,[36] 1.9 to 1.2,[37] and 1.5 to 1.0,[37] for different polydisperse LCB PE products as increases.

This manuscript summarizes a systematic computational investigation of trifunctional HP structural variants to clarify the relationship of $[\eta]$ and R_g to the Wiener index (W), where W is a quantitative measure of topology that can be

TABLE I. Degrees of polymerization, N, degrees of branching, DB, and Wiener indices, W, of all symmetric HPs. Extrapolated zero-shear intrinsic viscosities, a_0, and radii of gyration, R_g, of all symmetric HPs (where simulated) are shown.

N	Degree of branching, DB	Wiener index, W	a_0 (dimensionless)	R_g
49	0.94	7686	265	⋯
55	0.83	11 376	332	⋯
67	0.68	19 332	410	2.73
103	0.91	50 400	701	⋯
115	0.81	70 788	936	3.27
211	0.90	287 460	1722	3.83
70	0.65	15 957	331	⋯
82	0.55	25 713	455	2.63
88	0.51	34 299	594	⋯
166	0.56	130 725	1032	⋯
178	0.52	171 201	1338	⋯
358	0.53	817 605	2429	4.09

applied to any structure. Section II presents simulation details dealing with the generation of the simulated structures, the simulation algorithm, and the background to analysis protocols used. Results are presented in Sec. III with a discussion and conclusion contained in Sec. IV.

II. DETAILS OF SIMULATION

A. Generation of molecular structures

The structures of the HPs simulated within this study fall into two groups. The smaller of the two groups consisted of symmetric structures derived from dendrimer molecules. These "symmetric HPs" were created by selectively extending some of the layers within a basic dendrimer structure by adding an additional linear bead between branching points. As a result, the symmetric HPs have higher N values and lower DB than those of the molecule on which they are based. Their Wiener indices are also higher than those of dendrimers with the same number of repeat units. Twelve variants of the structures were generated based on dendrimers of generation 3, 4, and 5. Although these HPs retain dendrimer symmetry, the decreased level of branching and nonuniform distribution of branch points are in common with less regular HPs. Examples of the structures are pictured in Fig. 1, labeled with N, DB, and W values. Dendrimer structures are included for comparison. DB and W data on all symmetric molecules simulated are located in Table I.

DB is defined for all molecules according to Holter *et al.*,[38]

$$\text{DB} = \frac{2D}{2D + L}. \qquad (2.1)$$

D is the number of fully branched ("dendritic") beads and L is the number of partially reacted ("linear") beads. The Wiener index is defined by the formula

$$\text{W} = \frac{1}{2} \sum_{j=1}^{N} \sum_{i=1}^{N} d_{ij}, \qquad (2.2)$$

DB = 0.8   DB = 0.4

DB = 0.80, LFM
W = 34511

DB = 0.40, LFM
W = 44872

DB = 0.80, MAX
W = 36350

DB = 0.40, MAX
W = 50150

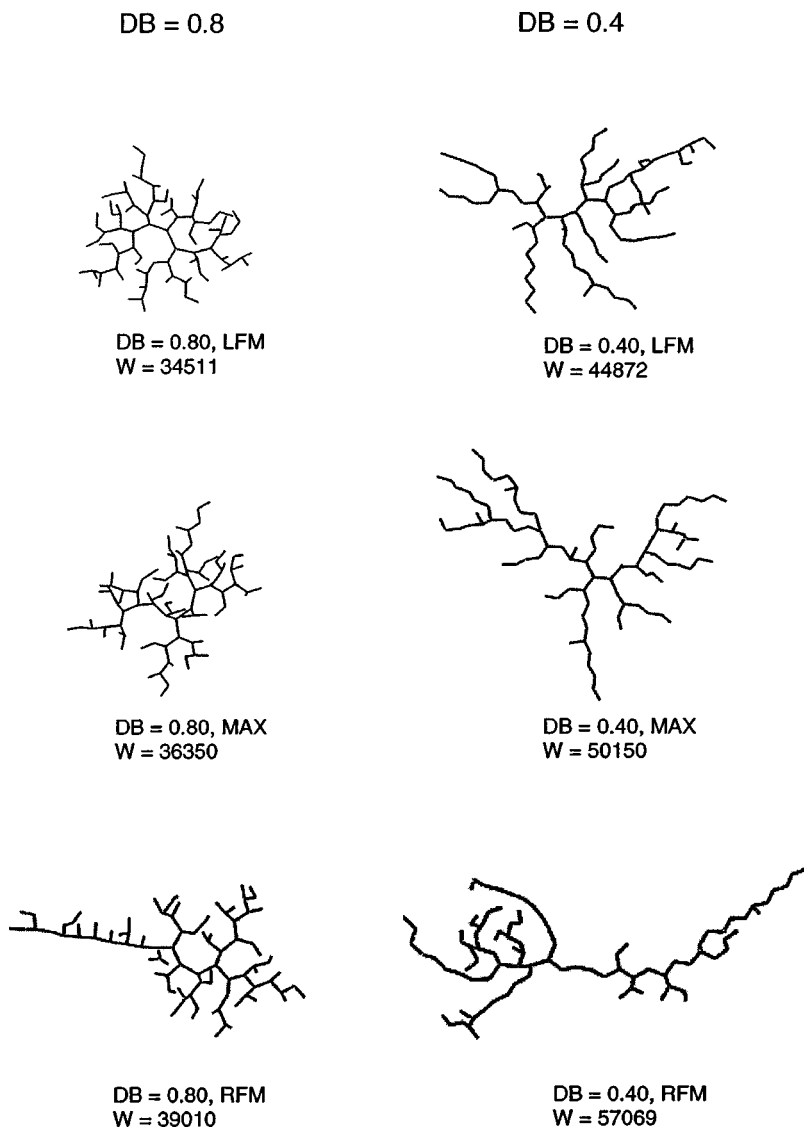DB = 0.80, RFM
W = 39010

DB = 0.40, RFM
W = 57069

FIG. 2. Structures of the 94-bead, DB=0.8 and DB =0.4 irregular hyperbranched molecules (HPs) simulated, labeled with Wiener indices, W.

where d_{ij} is the number of bonds separating the beads i and j of the structure, counted along the shortest path between them. However, W was calculated for all structures using an equivalent, more computationally efficient formula, which is applicable to molecules without loops,[13]

$$W = \sum_{s=1}^{N-1} (V_{L,s} \times V_{R,s}). \tag{2.3}$$

This sums the product of the number of vertices (beads) to the right (R) and left (L) of the center of each bond, s.

The main group of HPs were irregular molecules resulting from the same sequential addition process used by Lyulin et al.[14] Within this group, the HPs had the same degree of polymerization (N) as dendrimers of generations 4, 5, and 6 (i.e., $N = 94$, 190, 382). Lyulin et al. revealed that simulated intrinsic viscosity values for these dendrimers peak near generation 5 ($N = 190$).[14,39] At each N, HP molecules with DB =0.4, 0.6, and 0.8 were specified. For each of these DBs, at each N, two to three molecules were created having distinct Wiener indices selected according to a systematic procedure (detailed below). Examples of irregular 94-bead HPs are illustrated in Fig. 2 labeled with their respective DB and W.

Table II contains DB and W data on all irregular HP molecules simulated.

In this figure, the less branched DB=0.4 molecules contain longer linear sections relative to the DB=0.8 molecules. Meanwhile, W expresses the positioning of the branch points. In higher W molecules at a given DB and N, the branch points are more dispersed relative to molecules with lower W, where the branch points are relatively localized. In Fig. 1, two molecules with very similar N (67 and 70) and DB (0.68 and 0.65) have highly distinct W values, despite the symmetry of both molecules. This again expresses the relative localization of branch points in the lower W molecule.

The structure of every molecule took the form of a "connectivity tree," specifying the bonded neighbors for each bead. For a symmetric HP, the generation of a connectivity tree for the desired structure is trivial. For the irregular HPs, complete detail of the process of generating trees is found within Ref. 13. In brief, starting from a trifunctional core, B_3, with three free "B" ends, the molecule is grown outward by sequential addition of trifunctional AB_2 monomers to available free ends until N have been added. Only A and B

TABLE II. Degree of branching, DB, structure label and Wiener index, W, of all irregular HPs. Extrapolated zero-shear intrinsic viscosities, a_0, and radii of gyration, R_g, of all irregular HPs. MAX, LFM and RFM refer to structures selected from the distribution maximum and the left-hand and right-hand one-fourth maxima, respectively.

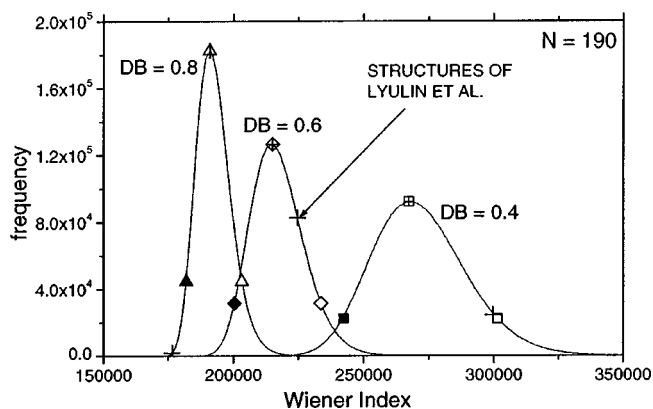| Degree of branching, DB	Structure	Wiener index, W	a_0	R_g
			(dimensionless)	
$N=94$				
0.4	RFM	57 069	877	3.65
	LFM	44 872	699	3.10
0.6	RFM	44 658	704	3.12
	MAX	40 600	633	3.01
	LFM	37 598	592	2.94
0.8	RFM	39 010	602	3.01
	MAX	36 350	571	2.91
	LFM	34 511	539	2.74
$N=190$				
0.4	RFM	300 889	2243	4.48
	LFM	242 210	1817	3.95
0.6	RFM	233 582	1748	3.92
	MAX	214 931	1604	3.74
	LFM	200 319	1472	3.63
0.8	RFM	203 132	1533	3.76
	MAX	190 772	1424	3.60
	LFM	181 812	1400	3.43
$N=382$				
0.4	RFM	1 504 085	4628	5.37
	LFM	1 241 169	3589	...
0.6	RFM	1 150 234	3513	4.88
	MAX	1 069 747	3211	4.54
	LFM	1 005 819	3103	4.44
0.8	RFM	1 002 350	3048	4.58
	MAX	949 116	3029	4.36
	LFM	908 370	2810	4.19

FIG. 3. Distributions of Wiener indices obtained at $N=190$ for each DB. Distributions for other N values are almost identical in appearance. Open, crossed, and filled symbols superimposed on each distribution represent RFM, MAX, and LFM structures, respectively. Squares denote DB=0.4, diamonds DB=0.6, and up-triangles DB=0.8. + denotes the W position of HP structures used by Lyulin *et al.* (Ref. 14). Dendrimers and linear molecules at $N=190$ have W values 160 893 and 1 143 135, respectively.

For each N and DB value, structures with W values corresponding to the maximum in the distribution and two additional structures on either side of the maximum at one-fourth the intensity of the maximum were saved for simulation. For DB=0.4, however, the "maximum" structures were not simulated. The structures are termed LFM (left one-fourth maximum), RFM (right one-fourth maximum) and MAX (maximum of the distribution) depending on the position their W value takes in the parent distribution. Data for these structures are denoted by filled, hollow, and crossed symbols, respectively, in all plots. Also, as in Fig. 3, the symbol shapes of square, diamond, and up-triangle are assigned to DB=0.4, 0.6, and 0.8 data, respectively. For fixed DB, the LFM structure possesses a lower W value than the RFM structure,

Cartesian coordinates of initial configurations were assigned to the beads of all the molecules according to a process by Murat and Grest.[41] In this process, beads are added sequentially from the core, in accordance with the connectivity tree, at a random orientation with respect to the parent bead to which they are bonded. This is repeated to build the entire molecule with conditions that (a) bonded pairs are rigidly separated by a bond length, l, and (b) nonbonded pairs of beads are separated by at least l. This prevents large pair forces disturbing the start of the simulation. If a given bead could not be added satisfying these conditions after 8000 attempts, the entire molecule was discarded and restarted.

B. Simulation algorithm

The molecules were simulated using Brownian dynamics. Submolecular structure was coarse grained so that the molecules consisted of spherical subunits ("beads") representing monomers joined to neighbors by freely rotating rigid bonds of length l. The following equation of motion[42] was employed

$$\vec{r}_i = \vec{r}_i^0 + \left(\frac{\Delta t}{kT}\right) \cdot \sum_j \mathbf{D}_{ij}^0 \cdot \vec{F}_j^0 + \vec{v}_i^0 \Delta t + \vec{\Phi}_i^0(\Delta t), \tag{2.5}$$

groups may react together, and cycles are not permitted. If one of the two free ends of a branch-terminated monomer reacts with a probability P_1, the reaction probability of its other free end is replaced by P_2. Applying this condition allows alteration of the resulting average DB, depending only on the ratio $\kappa = P_2/P_1$ as follows:[13,40]

$$\text{DB} = \frac{4}{3 + \sqrt{(\kappa+8)/\kappa}}. \tag{2.4}$$

By use of the appropriate κ values, large numbers (5×10^6 to 1×10^7) of different structures were generated at target DBs of 0.4, 0.6, and 0.8, and their Wiener indices, W, recorded. The recorded W values formed a distribution at each target DB, as shown in Fig. 3. This shows that W takes many values at the same DB at constant N. However, specifying DB localizes the range of possible W values a HP may have at a given N.

where i and j represent different beads from 1 to N. $\vec{r}_i^0$ is the position vector of bead i before a BD step Δt (superscript ^{0} represents prestep quantities), k is Boltzmann's constant and T is the simulated temperature. $\mathbf{D}_{ij}^0$ is the diffusion tensor while $\vec{F}_j^0$ represents interbead forces. $\vec{v}_i^0$ is the solvent velocity at the position x_i^0, y_i^0, z_i^0 of bead i due to steady shear of the system, where $v_{ix}^0 = y_i^0 \dot{\gamma}$; $v_{iy}^0 = v_{iz}^0 = 0$. $\dot{\gamma}$ is the dimensionless shear rate.

The solvent is represented as a structureless continuum with chain-solvent collisions mimicked by the vector $\vec{\Phi}_i^0(\Delta t)$ which has a zero mean and a variance–covariance matrix given by

$$\langle \vec{\Phi}_i^0(\Delta t) \vec{\Phi}_j^0(\Delta t) \rangle = 2\Delta t D_{ij}^0. \tag{2.6}$$

The diffusion tensor has diagonal elements,

$$D_{ii}^{(\alpha\beta)0} = \left(\frac{kT}{\zeta}\right)\delta_{\alpha\beta}, \quad i=0,...,N, \tag{2.7}$$

where α and β represent the x, y, or z components and $\delta_{\alpha\beta}$ is the Kronecker symbol. ζ is the translational coefficient of friction of each bead with the solvent defined as $\zeta = 6\pi\eta_s a$, where η_s is the solvent viscosity and a is the Stoke's hydrodynamic radius of a bead. The off-diagonal elements of D_{ij}^0 represent the hydrodynamic interactions (HI) between beads. These are calculated rigorously according to the Rotne–Prager–Yamakawa interaction tensor,[42]

$$D_{ij}^{(\alpha\beta)0} = h* \left(\frac{\pi}{3}\right)^{1/2} \left(\frac{3kT}{4\zeta}\right)\left(\frac{l}{R_{ij}}\right)\left[\left(\delta_{\alpha\beta} + \frac{R_{ij}^\alpha R_{ij}^\beta}{R_{ij}^2}\right)\right.$$
$$\left. + \frac{2a^2}{3R_{ij}^2}\left(\delta_{\alpha\beta} - \frac{3R_{ij}^\alpha R_{ij}^\beta}{R_{ij}^2}\right)\right]. \tag{2.8}$$

R_{ij} is the separation of beads i and j. $h*$ sets the strength of the HI, where

$$h* = \left(\frac{3}{\pi}\right)^{1/2}\left(\frac{a}{l}\right). \tag{2.9}$$

A value of $h* = 0.25$ is used with the simulation which corresponds to a bead hydrodynamic radius $a = 0.257l$.[39] For overlapping beads, Eq. (2.8) is rewritten,[43]

$$D_{ij}^{(\alpha\beta)0} = \left(\frac{kT}{\zeta}\right)\left[\left(1 - \frac{9R_{ij}}{32a}\right)\delta_{\alpha\beta} + \left(\frac{3}{32a}\right)\frac{R_{ij}^\alpha R_{ij}^\beta}{R_{ij}^2}\right]. \tag{2.10}$$

The direct interbead forces are represented by $\vec{F}_j^0$,

$$\vec{F}_j^0 = -\sum_{k=1}^N \lambda_k \left(\frac{\partial \sigma_k}{\partial \vec{r}_j}\right)_{r^0} - \frac{\partial U_{LJ}}{\partial \vec{r}_j^0}. \tag{2.11}$$

σ_k is an equation of rigid constraint for the kth bond, and λ_k is the corresponding Lagrange multiplier. A modified version of the SHAKE[44] algorithm due to Allison and McCammon[45] is employed.

The second term on the right of Eq. (2.11) represents the forces between nonbonded beads i and j, expressed by a Lennard-Jones potential,

$$U_{LJ} = \sum_{ij} 4\varepsilon\left(\left(\frac{\sigma}{R_{ij}}\right)^{12} - \left(\frac{\sigma}{R_{ij}}\right)^6\right). \tag{2.12}$$

A cutoff was imposed for this potential at a separation of 2.5σ. No valence or torsion angle potentials were employed. An ε value of $0.3kT$ and a σ value of $0.8l$ were used as proposed by Rey and co-workers[46] to reproduce the mean-square end-to-end length of a linear chain in θ-solution. Dimensionless reduced units were employed such that $l=1$, $kT=1$, and $\zeta=1$. Hence, time is reduced by $\zeta l^2/kT$ and shear rate by $kT/\zeta l^2$. Quantities from this point onward are expressed in these units unless otherwise stated. Minimum and maximum dimensionless shear rates of $\dot{\gamma}=0.024$ and 1.2 were used with dimensionless time-steps of 4×10^{-4} and 2×10^{-4}, respectively, for $N=94$ irregular HP molecules. For irregular $N=190$ and 382 molecules, $\dot{\gamma}=0.006$ and 0.6 were the minimum and maximum dimensionless shear rates, using dimensionless time-steps of 6×10^{-4} and 4×10^{-4}, respectively. Similar parameters were used for the symmetric HPs with the $\dot{\gamma}$ range depending on size while time-step was decreased for higher shear rates and smaller molecules. These parameters are in keeping with work of Lyulin et al. on similar molecules.[14,39] Simulation runs of 3×10^5 to 1×10^6 time-steps were used for equilibration, depending on molecular size. Typically, production runs spanned 2×10^7 steps for $N=94$ molecules, 1×10^7 to 2×10^7 steps for $N=190$ molecules, and 3×10^6 to 6×10^6 steps for $N=382$ molecules. This translates to runs at low N values requiring one or two days of Origin 2000 CPU time whereas the lower shear rate $N=382$ systems required four months of CPU time on the same platform. Additional simulations were carried out to obtain average dimensionless radii of gyration (R_g) in the absence of shear. Here, the same time-step and equilibration length were used as for the lowest finite shear simulation of a given molecule, with R_g data being sampled from up to 2×10^6 steps of subsequent production. Further simulation details can be found in the work of Lyulin et al.[47] Error bars in all plots are smaller than the size of the data symbols used and lines on graphs are guides to the eye, unless otherwise indicated.

C. Processing of results

1. Viscosity

The simulated intrinsic viscosity[39] was calculated according to the following expression,

$$[\eta]* = \frac{(\eta - \eta_s)}{nkT\lambda}, \tag{2.13}$$

where λ is the characteristic time of orientational diffusion of a single monomer,[39] η is the shear viscosity, η_s is the viscosity of the solvent, and n is the number density of molecules. The shear viscosity was obtained through the nondiagonal component of the shear stress,

$$\eta = -\frac{\tau_{xy}}{\dot{\gamma}}. \tag{2.14}$$

Figure 4 shows the shear thinning behavior at high shear rate for a selection of the molecules studied. Similar shear thinning has been reported previously for dendrimer[39] and HP[14] molecules. A Newtonian plateau exists, facilitating extrapolation to zero shear-rate to afford the zero shear intrinsic
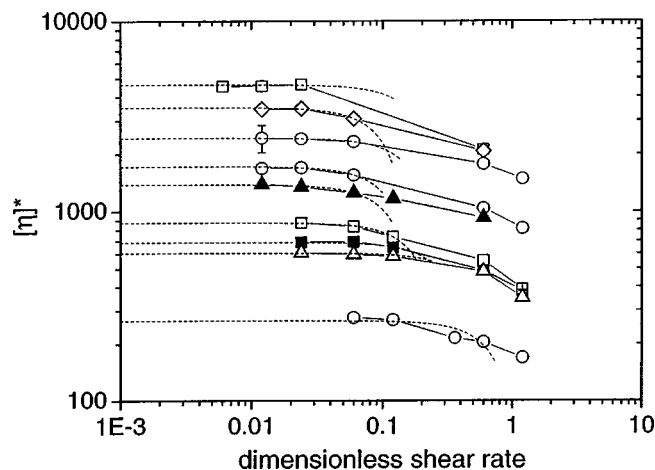
FIG. 4. Simulated intrinsic viscosity vs shear rate for a selection of HPs of differing degrees of polymerization (N) and structure. Circles denote symmetric HPs. Other symbols represent irregular HPs where squares denote DB=0.4, diamonds DB=0.6, and up-triangles DB=0.8. Open symbols and filled symbols represent RFM and LFM structures, respectively. Dashed lines indicate quadratic extrapolations to zero shear from the lowest three to four shear rate points to obtain a_0 values recorded in Tables I and II.

viscosity. The extrapolation process used to extract the zero shear intrinsic viscosity employs at least three of the lowest shear rate data points per molecule and the equation,

$$[\eta]^* = a_0 - a_1\dot{\gamma}^2, \tag{2.15}$$

where a_0 is the zero shear intrinsic viscosity.[39] This form is justified since the intrinsic viscosity does not depend on the direction of the shear and the intrinsic viscosity decreases with increasing shear rate (i.e., shear thinning). Values of a_0 are found in Tables I and II for the symmetric and irregular HPs, respectively. The experimental intrinsic viscosity uses a concentration rather than a number density of molecules within its definition. Translation of the data defined by Eq. (2.13) into a quantity consistent with an experimental intrinsic viscosity is accomplished by introducing $[\tilde{\eta}] = a_0/N$. This procedure was followed for all simulated molecules to produce the intrinsic viscosity data within Figs. 5–8.

2. Hydrodynamic radius

A hydrodynamic radius (R_h) for a HP can be obtained through the diffusion coefficient via mean-squared displacement data. However, Lyulin et al.[14] report R_h values for HPs computed in this manner are quantitatively similar to R_h values computed via

$$R_h = \left(\frac{3N[\tilde{\eta}]}{10\pi}\right)^{1/3}. \tag{2.16}$$

R_h values within this manuscript are computed using Eq. (2.16).

III. RESULTS

A. Comparison of HPs to dendrimers

Figures 5(a)–5(c) illustrate the variation of the zero shear intrinsic viscosity with N. LFM and RFM structures for each DB are shown and MAX structures have been omitted
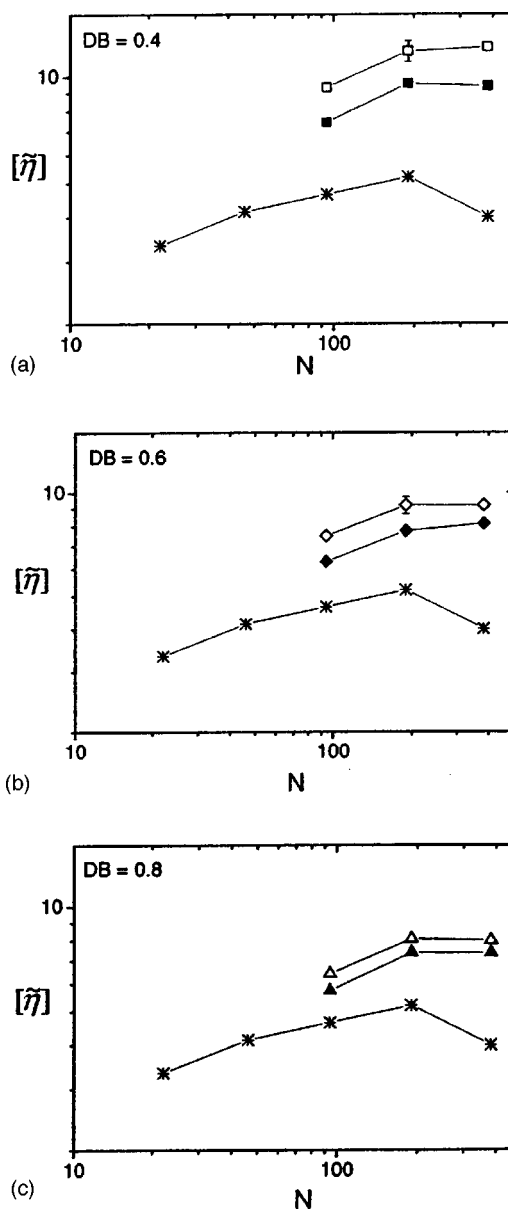

FIG. 5. $[\tilde{\eta}]$ vs N for irregular HPs at constant DB in comparison to dendrimers. Open symbols and filled symbols represent RFM and LFM structures, respectively. Squares denote DB=0.4, diamonds DB=0.6, up-triangles DB=0.8, and asterisks denote dendrimer data.

for the sake of clarity. The simulated data for the corresponding dendrimers of Lyulin et al. are included, but Lyulin's HP data are not displayed as they do not represent a consistent specification of W.

Figures 5(a)–5(c) reveal that $[\tilde{\eta}]$ values for the HPs are substantially higher than the corresponding denrimer $[\tilde{\eta}]$ values. Also, at a given DB and N, RFM structures (open symbols) have higher $[\tilde{\eta}]$ than LFM structures (filled symbols). This corresponds with the higher W of the RFM structures, emphasizing the sensitivity of $[\tilde{\eta}]$ to molecular compactness at the same DB.

The HP curves in each panel of Fig. 5 reflect a peak or plateau in $[\tilde{\eta}]$ at N values where a definite peak in the dendrimer $[\tilde{\eta}]$ is observed. Within each curve, the difference in $[\tilde{\eta}]$ at $N=190$ and $N=382$ is small compared to the
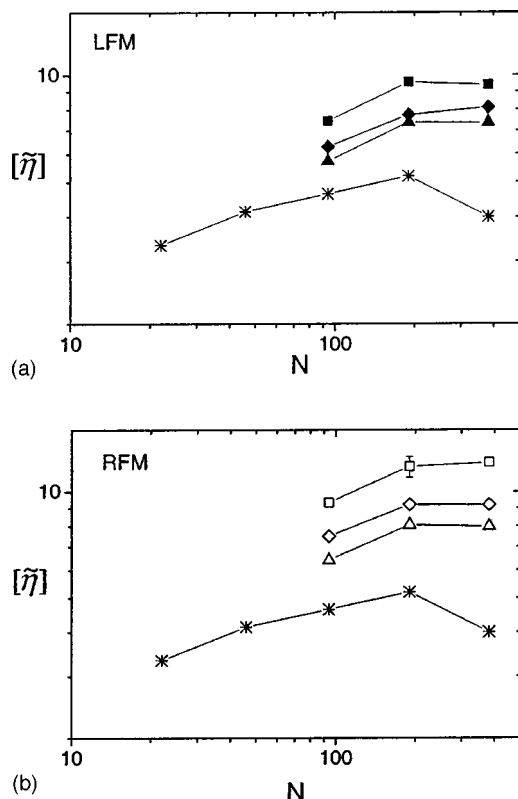
(a)

(b)

FIG. 6. $[\tilde{\eta}]$ vs N data for HPs selected from the same part of the parent W distribution. Filled and open symbols represent LFM and RFM structures, respectively. Squares denote DB=0.4, diamonds DB=0.6, up-triangles DB =0.8, and asterisks denote dendrimers.

strength of the W dependence at DB=0.6 and 0.4. Hence for a given DB, if one structure is chosen at each N without regard to its W value, the evidence of a peak in $[\tilde{\eta}]$ with increasing N is easily accentuated or eliminated. For example, if in Fig. 5(a) at $N=94$ and $N=190$, the DB=0.4 LFM structures are selected with the DB=0.4 RFM structure used at $N=382$, an apparent scaling of $[\tilde{\eta}]$ with N results. Alternatively, taking the LFM structures of Fig. 5(a) at $N =94$ and $N=382$, with the RFM structure at $N=190$ would reveal a significant peak in $[\tilde{\eta}]$ versus N. At DB=0.8, the
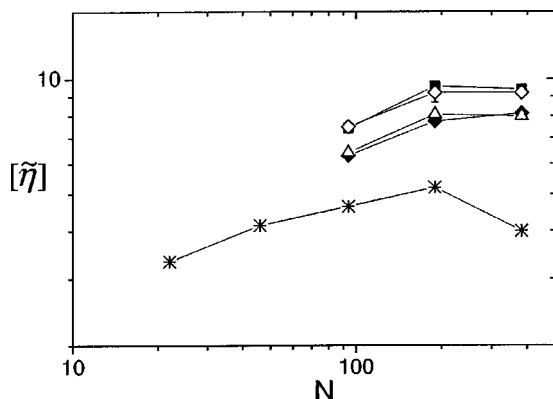

FIG. 7. $[\tilde{\eta}]$ vs N illustrating the overlap of various LFM and RFM data sets. Squares denote DB=0.4, diamonds DB=0.6, and up-triangles DB=0.8. Open symbols and filled symbols represent RFM and LFM structures, respectively. Asterisks denote dendrimers.
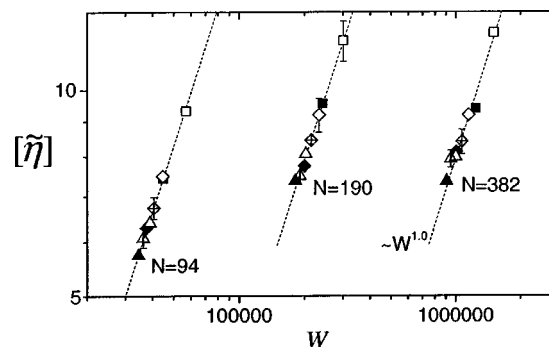

FIG. 8. Correlation of $[\tilde{\eta}]$ with Wiener index, W, for irregular HPs. All DBs are shown. Squares denote DB=0.4, diamonds DB=0.6, and up-triangles DB=0.8. Open, crossed, and filled symbols represent RFM, MAX, and LFM structures, respectively. Dotted lines indicate a fit using $[\tilde{\eta}]\sim W^a$ for each N with the exponents reported in Table III.

qualitative $[\tilde{\eta}]$ behavior is more resilient to Wiener index variation, since a narrower range of $[\tilde{\eta}]$ is explored by structures with different W [Fig. 5(c)].

Figure 6 shows that $[\tilde{\eta}]$ increases with decreasing DB if the Wiener index is consistently specified as LFM [Fig. 6(a)] or RFM [Fig. 6(b)]. The difference between adjacent DBs in Fig. 6(a) or 6(b) is comparable to the interval in Figs. 5(a)–5(c) between LFM and RFM structures at the same DB. This means that substantially different DB molecules with the same N may have the same $[\tilde{\eta}]$ depending on the choice of Wiener index. Figure 7 illustrates this point where RFM points of DB=0.8 virtually overlay with LFM points of DB =0.6. DB=0.4 and 0.6 show a similar overlap.

B. Comparison of intrinsic viscosity and radius of gyration with Wiener index

As discussed previously, the literature supports a power law correlation of $[\eta]$ with W and of R_g with W for a given degree of polymerization, N. Up to now, simulations have focused on the dependence of HP intrinsic viscosities on DB at a given N. For the present study, simulations were performed to allow the independent determination of both $[\tilde{\eta}]$ and R_g of HP molecules, with a range of W at each N value, chosen systematically at different DBs.

1. Intrinsic viscosity

The $[\tilde{\eta}]$ values from Fig. 5 are plotted against W in Fig. 8. A power law relationship of the form

$$[\tilde{\eta}]\sim W^a \quad (3.1)$$

clearly exists for each set of data where N is held constant, as was observed in the previous efforts.[13,14]

The three groups representing different N values in Fig. 8 involve structures with different DBs. All data in each group fall onto a single line. DB does not therefore play a quantitative role in setting the value of $[\tilde{\eta}]$. However, DB localizes W at constant N (see Fig. 3), placing limits on the value $[\tilde{\eta}]$ can take.

Fitting Eq. (3.1) to the data within the $N=94$, $N=190$, and $N=382$ systems in turn yields values of $a=1.0$ in every case within error (see Table III). The separation of the groups

TABLE III. Exponents in the power law relationships $[\tilde{\eta}] \sim W^a \times N^b$ and $R_g \sim W^c \times W^d$. a and c are obtained from fits for irregular HPs at constant N. b and d are obtained from fits for all HPs after setting c to 0.5 and a to 1.0.

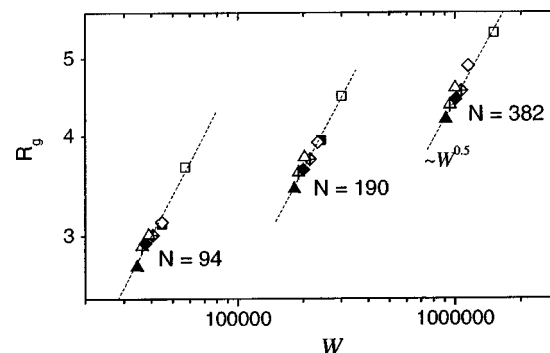| N	a	c
94	0.99±0.04	0.52±0.03
190	0.99±0.03	0.51±0.02
382	1.00±0.02	0.50±0.03
	b	d
All	−2.20±0.01	−0.85±0.01

FIG. 10. Correlation of R_g with W for irregular HPs. All DBs are shown. Squares denote DB=0.4, diamonds DB=0.6, and up-triangles DB=0.8. Open, crossed, and filled symbols represent RFM, MAX, and LFM structures, respectively. Dotted lines correspond to a fit using $R_g \sim W^c$ at each N value with the exponents reported in Table III.

by N is indicative of an N dependence, which is added to Eq. (3.1) following Widmann and Davies as

$$[\tilde{\eta}] \sim W^a \times N^b. \tag{3.2}$$

The bare N dependence is obtained as,

$$\frac{[\tilde{\eta}]}{W} \sim N^b, \tag{3.3}$$

where a has been set to 1.0. The $[\tilde{\eta}]$ data of Fig. 6 were recalculated as the left-hand side of Eq. (3.3), and plotted versus N as shown in Fig. 9.

The data are observed to collapse onto a single line. Points can be seen in Fig. 9 in between the discrete-dendrimer-equivalent N values of 94, 190, and 382. These data were calculated from simulations of the symmetric HP structures introduced earlier. Fitting all of the data to Eq. (3.3) allows the determination of the second exponent of Eq. (3.2) as $b = -2.20 \pm 0.01$, affording the final relationship

$$[\tilde{\eta}] \sim W^{1.0} \times N^{-2.2}. \tag{3.4}$$

2. Radius of gyration

R_g data were obtained for the HP molecules by performing simulations in the absence of shear. Values of R_g are located in Tables I and II. Scaling of R_g with W is investigated for HPs using the simulated R_g values, following a similar approach to the previous section.

The plots of R_g data versus W in Fig. 10 are qualitatively similar to the plots of $[\tilde{\eta}]$ versus W in Fig. 8. For each data set grouped by N, a power law relationship of the form

$$R_g \sim W^c \tag{3.5}$$

is clearly observed. Fitting each group of data with Eq. (3.5) affords a c value of 0.5 for all three cases within error (see Table III). The increase of R_g with W at constant N is expected, since a higher W molecule should be less compact than a molecule with a lower W. The N dependence is incorporated into Eq. (3.5) as

$$R_g \sim W^c \times N^d \tag{3.6}$$

in the spirit of Eq. (3.2). The R_g data were recalculated according to the left-hand side of Eq. (3.7) obtained by setting c to 0.5 in Eq. (3.6),

$$\frac{R_g}{W^{0.5}} \sim N^d, \tag{3.7}$$

and plotted in Fig. 11 versus N.

The data are observed to collapse onto a single line with a slope of $d = -0.85 \pm 0.01$. Again, data from simulations of the symmetric HPs are included within this plot. In light of Figs. 10 and 11, a relationship between R_g, W, and N for all of the molecules considered can be cast as

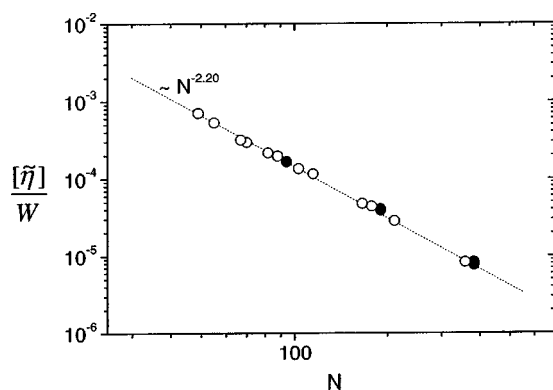$$R_g \sim W^{0.5} \times N^{-0.85}. \tag{3.8}$$

FIG. 9. Correlations of $[\tilde{\eta}]$/W with N. Symmetric (open symbols) and irregular (filled symbols) HPs are shown. The dotted line indicates a fit of the data using $[\tilde{\eta}]/W \sim N^b$ which yields $b = -2.20 \pm 0.01$.
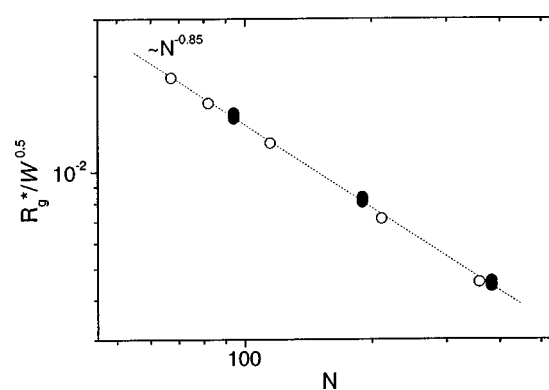

FIG. 11. Correlation of R_g/W$^{0.5}$ with N. Symmetric (open symbols) and irregular (filled symbols) HPs are shown. The dotted line indicates a fit of the form $R_g/W^{0.5} \sim N^d$ affording $d = -0.85 \pm 0.01$.

The fitted exponents of Eqs. (3.4) and (3.8) are empirical, but reflect the sensitivity of $[\tilde{\eta}]$ and R_g of highly branched molecules to topology via W and to the number of repeat units, N. This contrasts with the simple N dependence of linear polymers.

3. Comparisons with other results

Equations (3.4) and (3.8) may be assessed in the light of other work. The theoretical value for the exponent in the power law relationship between R_g and W was reported earlier as 0.5^{21} and is in excellent agreement with current findings (see Table III). An analytically predicted exponent of 1.5^{13} in the power law relationship between $[\eta]$ and W is higher than the finding from this study which places this value around 1.0 (see Table III). However, the analytical method used the relationship $[\eta] \sim R_g^{\,3}$, in a limiting case for hard uniform spheres. In contrast, the present results for $[\eta]$ and R_g were obtained by independent methods from solution state simulations. Widmann and Davies' RMMC work generated higher exponents of $a = 2.7$ to 2.1, $c = 0.9$ to 0.7, whose deviations above the theoretical values were rationalized in terms of shortcomings of the model, which used phantom chains without solvent or HI[13]. The BD work of Lyulin et al. found $a = 1.2$ to 1.1 for $N = 94$ to 382, agreeing with the values found in this work within error.[14]

In a recent Brownian dynamics simulation by Lee and McHugh using phantom chains and trumbell-FENE spring subunits, zero shear viscosities of HPs were correlated with the average number of unbranched units between branch points.[48] However, several pairs or triplets of molecules were simulated, in which each molecule had the same number of branch units and the same degree of polymerization (or equivalently the same DB and N), but different branching arrangements (i.e., different W). Members within each pair or triplet were found to have viscosity values varying up to 25%.[48]

4. Molecular conformation

The ratio R_g/R_h is related to molecular conformation, having a value 1.504 for ideal linear polymers and 0.775 for hard uniform spheres respectively. Its value is found to vary strongly for different branched polymers.[24,25] Simulations and experiments reveal dendrimers exhibit ratios near or below the sphere value, especially at higher generations.[24,49,50] Furthermore, dendrimers' radial density distribution in solution becomes more like that of a uniform sphere with increasing generation number.[39,41,49,51–53] R_g/R_h ratios are plotted in Fig. 12 for the simulated irregular HP molecules. Dotted and solid lines represent the values for linear ideal chains and hard uniform spheres, respectively.

The simulated molecules straddle the value 1.00. The ratio decreases toward the spherelike value overall as N increases. Also, R_g/R_h decreases at a given N value as W decreases, suggesting a more compact branching configuration leads to a more compact conformation. This underlines the importance of an approach encompassing the Wiener index when considering the conformation of HP molecules.
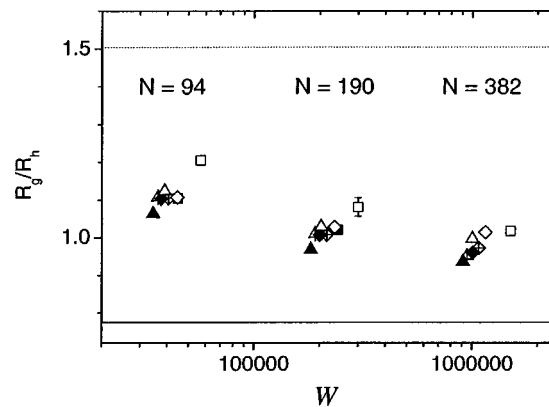

FIG. 12. Ratio of radius of gyration to hydrodynamic radius, R_g/R_h, vs Wiener index, W, for the irregular HPs. Squares denote DB=0.4, diamonds DB=0.6, and up-triangles DB=0.8. Open, crossed, and filled symbols represent RFM, MAX, and LFM structures, respectively. Values of 0.775 for a hard, uniform sphere (solid) and 1.504 for an unperturbed linear chain (Ref. 29) are shown for comparison.

IV. DISCUSSION AND CONCLUSION

A. Direct relationship between intrinsic viscosity and radius of gyration

Equations (3.4) and (3.8) allow $[\tilde{\eta}]$ and R_g to be related through the elimination of either W or N. This process affords

$$[\tilde{\eta}] \sim R_g^{2.6} \times W^{-0.3}, \tag{4.1}$$

$$[\tilde{\eta}] \sim R_g^{2} \times N^{-0.5}, \tag{4.2}$$

which apply to both the symmetric and irregular HPs.

Zimm and Kilb proposed $g' \approx g^{0.5}$ for the intrinsic viscosity and radius of gyration contraction factors of branched polymers. Before this, Thurmond and Zimm compared the intrinsic viscosity of branched and linear polymers, using Eq. (1.1) for the branched molecules,[32] which implies[31] $g' = g^{1.5}$. A relation of g and g' may be constructed for the present HPs. Equation (4.2) expresses their intrinsic viscosities, $[\tilde{\eta}]_{HP}$. Furthermore, Eq. (1.1) is assumed to apply to the intrinsic viscosity, $[\tilde{\eta}]_L$, and the radius of gyration, R_{gL}, of linear molecules. Thus, at a constant N,

$$\frac{[\tilde{\eta}]_{HP}}{[\tilde{\eta}]_L} \sim \frac{R_{gHP}^{2} N^{-0.5}}{R_{gL}^{3} N^{-1}} \sim \frac{R_{gHP}^{2}}{R_{gL}^{3} N^{-0.5}}. \tag{4.3}$$

Assuming $R_{gL} \sim N^{0.5}$ for a θ-solution of linear molecules, Eq. (4.3) simplifies to

$$\frac{[\tilde{\eta}]_{HP}}{[\tilde{\eta}]_L} \sim \frac{R_{gHP}^{2}}{R_{gL}^{2}}, \tag{4.4}$$

reflecting $g' = g^{1.0}$. This exponent value of 1.00 is within the range 0.5–2.0 found experimentally for LCB PE[37] and falls centrally between the two theoretical predictions for polymers.

B. Conclusion

The dependence of intrinsic viscosity on N for HPs has traditionally been investigated by the use of a range of structures with different DB and N. This reveals that HPs have $[\eta]$

values which are lower than linear molecules of the same N and higher than dendrimers of the same N. Higher DB molecules are found to have $[\eta]$ values closer to those of corresponding dendrimers, relative to lower DB molecules.[11,13,14] This investigation reveals an important dependence of $[\tilde{\eta}]$ on W at a given N. A systematic approach to W yielded results which reflect a peak or plateau in $[\tilde{\eta}]$ of HPs as N increases. The analysis carried out illustrates that without a strict specification of W at each N when initially selecting HP structures, the results at a given DB could easily exhibit a significant dendrimerlike peak in $[\tilde{\eta}]$ with increasing N, or a linear polymerlike $[\tilde{\eta}] \sim N^{\alpha}$ behavior. The empirical relationships obtained in this study for HPs are based on systems which are monodisperse in N, DB, and W. Future investigations will tackle systems polydisperse in one or more of these parameters.

ACKNOWLEDGMENTS

[1] D. A. Tomalia, A. M. Naylor, and W. A. Goddard, Angew. Chem. Int. Ed. Engl. **29**, 138 (1990).
[2] J. M. J. Fréchet, C. J. Hawker, I. Gitsov, and J. W. Leon, J. Macromol. Sci., Pure Appl. Chem. **A33**, 1399 (1996).
[3] Y. H. Kim, J. Polym. Sci. A **36**, 1685 (1998).
[4] B. I. Voit, J. Polym. Sci. A **38**, 2505 (2000).
[5] T. H. Mourey, S. R. Turner, M. Rubinstein, J. M. J. Frechet, C. J. Hawker, and K. L. Wooley, Macromolecules **25**, 2401 (1992).
[6] L. J. Hobson and W. J. Feast, Chem. Commun. (Cambridge) **21**, 2067 (1997).
[7] E. T. F. Gelade, B. Goderis, C. G. de Koster, N. Meijerink, R.A. T. M. van Benthem, R. Fokkens, N. M. M. Nibbering, and K. Mortensen, Macromolecules **34**, 3552 (2001).
[8] D. Parker and W. J. Feast, Macromolecules **34**, 2048 (2001).
[9] S. R. Turner, B. I. Voit, and T. H. Mourey, Macromolecules **26**, 4617 (1993).
[10] S. R. Turner, F. Walter, B. I. Voit, and T. H. Mourey, Macromolecules **27**, 1611 (1994).
[11] J. Aerts, Comput. Theor. Polym. Sci. **8**, 49 (1998).
[12] R. M. Lescanec and M. Muthukumar, Macromolecules **23**, 2280 (1990).
[13] A. H. Widmann and G. R. Davies, Comput. Theor. Polym. Sci. **8**, 191 (1998).
[14] A. V. Lyulin, D. B. Adolf, and G. R. Davies, Macromolecules **34**, 3783 (2001).
[15] H. Wiener, J. Am. Chem. Soc. **69**, 17 (1947).

[16] D. H. Rouvray, Math. Chem. (MATCH) **1**, 125 (1975).
[17] D. H. Rouvray and S. S. Crafford, Afr. J. Sci. **72**, 47 (1976)
[18] D. Bonchev, O. Mekenyan, and V. Kamenska, Math. Chem. (MATCH) **11**, 107 (1992).
[19] I. Gutman, Y-N. Yeh, S. L. Lee, and Y-L. Luo, Ind. J. Chem. **32A**, 651 (1993).
[20] D. Bonchev and N. Trinajstić, J. Chem. Phys. **67**, 4517 (1977).
[21] D. Bonchev, E. J. Markel, and A. H. Dekmezian, Polymer **43**, 203 (2002).
[22] K-H. Nitta, J. Chem. Phys. **101**, 4222 (1994).
[23] P. J. Flory and T. G. Fox, Jr., J. Am. Chem. Soc. **73**, 1904 (1951).
[24] B. M. Tande, N. J. Wagner, M. E. Mackay, C. J. Hawker, and M. Jeong, Macromolecules **34**, 8480 (2001).
[25] B. J. Bauer, L. J. Fetters, W. W. Graessley, N. Hadjichristidis, and G. F. Quack, Macromolecules **22**, 2337 (1989).
[26] J. Roovers, L.-L. Zhou, P. M. Toporowski, M. van der Zwan, H. Iatrou, and N. Hadjichristidis, Macromolecules **26**, 4324 (1993).
[27] M. Schmidt, D. Nerger, and W. Burchard, Polymer **20**, 582 (1979).
[28] M. Antonietti, W. Bremser, and M. Schmidt, Macromolecules **23**, 3796 (1990).
[29] W. Burchard, Adv. Polym. Sci. **143**, 113 (1999).
[30] B. H. Zimm and W. H. Stockmayer, J. Chem. Phys. **17**, 1301 (1949).
[31] B. H. Zimm and R. W. Kilb, J. Polym. Sci. **37**, 19 (1959).
[32] C. D. Thurmond and B. H. Zimm, J. Polym. Sci. **5**, 477 (1952).
[33] M. Kurata, M. Abe, M. Imwama, and M. Matsushima, Polym. J. (Tokyo) **3**, 729 (1972).
[34] G. R. Meira, *Modern Methods of Polymer Characterization* (Wiley, New York, 1991).
[35] V. R. Kuhn, H. Krömer, and G. Rosmanith, Angew. Makromol. Chem. **40−41**, 361 (1974).
[36] T. G. Scholte, *Developments in Polymer Characterization, Vol. 4* (Applied Science, Essex, 1984).
[37] P. Tackx and J. C. J. F. Tacx, Polymer **39**, 3109 (1998).
[38] D. Hölter, A. Burgath, and H. Frey, Acta Polym. **48**, 30 (1997).
[39] A. V. Lyulin, G. R. Davies, and D. B. Adolf, Macromolecules **33**, 3294 (2000).
[40] D. Hölter and H. Frey, Acta Polym. **48**, 298 (1997).
[41] M. Murat and G. S. Grest, Macromolecules **29**(4), 1278 (1996).
[42] D. L. Ermak and J. A. McCammon, J. Chem. Phys. **69**, 1352 (1978).
[43] J. Rotne and S. Prager, J. Chem. Phys. **50**, 4831 (1969).
[44] J.-P. Ryckaert and A. Bellemans, Chem. Phys. Lett. **30**, 123 (1975).
[45] S. A. Allison and J. A. McCammon, Biopolymers **23**, 167 (1984).
[46] A. Rey, J. J. Friere, and J. G. de la Torre, Macromolecules **20**, 2385 (1987).
[47] A. V. Lyulin, D. B. Adolf, and G. R. Davies, J. Chem. Phys. **111**, 758 (1999).
[48] A. T. Lee and A. J. McHugh, Macromolecules **34**, 7127 (2001).
[49] R. Scherrenberg, B. Coussens, P. van Vliet, G. Edouard, J. Brackman, and E. de Brabander, Macromolecules **31**, 456 (1998).
[50] I. B. Rietveld and J. A. M. Smit, Macromolecules **32**, 4608 (1999).
[51] M. L. Mansfield and L. I. Klushin, Macromolecules **26**, 4262 (1993).
[52] K. Karatasos, D. B. Adolf, and G. R. Davies, J. Chem. Phys. **115**, 5310 (2001).
[53] T. J. Prosa, B. J. Bauer, E. J. Amis, D. A. Tomalia, and R. Scherrenberg, J. Polym. Sci. **35**, 2913 (1997).